JP Journal of Heat and Mass Transfer

Available online at http://pphmj.com/journals/jphmt.htm
Volume 10, Number 1, 2014, Pages 1-32

REDUCED MODELS FOR COUPLED HEAT AND MOISTURE TRANSFER SIMULATION IN WOOD WALLS

E. Palomo del Barrio, S. Raji, M. Duquesne and A. Sempey

Université de Bordeaux
Institut de Mécanique et d'Ingénierie-Bordeaux
UMR CNRS 5295, I2M - Site AMPT
Esplanade des Arts et Métiers, 33405 Talence
France
e-mail: marie.duquesne@u-bordeaux.fr

Abstract

A method for accurate description of coupled heat and mass transfer phenomena within wood-walls using linear, low-dimensional models has been proposed. The partial differential equations that describe the hydrothermal behaviour of the wall are first linearized, thus decoupled and finally reduced to a very low number of ordinary differential equations using a powerful method based on singular valued decomposition techniques. Progressive empirical and numerical validation illustrates the quality of the results.

Nomenclature

c_l Specific heat of water in liquid state $(\mathrm{J.kg^{-1}.K^{-1}})$

c_s Specific heat of the wood solid matrix $(\mathrm{J.kg^{-1}.K^{-1}})$

Received: February 13, 2014; Accepted: June 3, 2014
Keywords and phrases: heat and moisture transfer, linearization, model reduction, buildings.

c_v Specific heat of water vapour $(\mathrm{J.kg^{-1}.K^{-1}})$

c Apparent specific heat $(\mathrm{J.kg^{-1}.K^{-1}})$

D_e Effective diffusivity of water vapour in the porous space $(\mathrm{m^2.s^{-1}})$

D_{Tl} Coefficient of water diffusion due to temperature gradients $(\mathrm{m^2.s^{-1}.K^{-1}})$

D_{Tv} Coefficient of water vapour diffusion due to temperature gradients $(\mathrm{m^2.s^{-1}.K^{-1}})$

D_{wl} Coefficient of water diffusion due to water content gradients $(\mathrm{m^2.s^{-1}})$

D_{wv} Coefficient of water vapour diffusion due to water content gradients $(\mathrm{m^2.s^{-1}})$

g Acceleration due to gravity $(\mathrm{m.s^{-2}})$

J_l Water liquid density flux $(\mathrm{kg.m^{-2}.s^{-1}})$

J_v Water vapour density flux $(\mathrm{kg.m^{-2}.s^{-1}})$

J_q Heat density flux $(\mathrm{W.m^{-2}})$

K_l Hydraulic conductivity $(\mathrm{m.s^{-1}})$

K_v Water vapour conductivity $(\mathrm{m.s^{-1}})$

Ko Kossovitch number (–)

L Wall thickness (m)

L_v Latent heat of water vaporization $(\mathrm{J.kg^{-1}})$

Lu Luikov number (–)

P Total pressure (Pa)

P_{vs} Saturated water vapour pressure (Pa)

Pn Possnov number (–)

R_v Gas constant of water vapour $(\mathrm{J.kg^{-1}.K^{-1}})$

T Temperature (K), $(^{\circ}\mathrm{C})$

t Time (s)

x Space coordinate (m)

w_l Water content (kg water/kg drymatter)

w_v Water vapour content (kg vapour/kg drymatter)

Greek letters

α Effective thermal diffusivity $(\mathrm{m^2.s^{-1}})$

α_m Diffusion coefficient of moisture $(\mathrm{m^2.s^{-1}})$

δ Thermogradient coefficient (–)

ε_a Gas volume fraction, porosity (–)

ε_l Liquid volume fraction (–)

ε_s Solid volume fraction (–)

φ Relative humidity (–)

λ_e Effective thermal conductivity $(\mathrm{W.m^{-1}.K^{-1}})$

λ Apparent thermal conductivity $(\mathrm{W.m^{-1}.K^{-1}})$

θ_1 Dimensionless temperature (–)

θ_2 Dimensionless water content (–)

ρ_l Water liquid density ($kg.m^{-3}$)

ρ_o Dry wood density ($kg.m^{-3}$)

τ Dimensionless time (–)

ψ Water potential (m)

1. Introduction

Living houses built in massive wood are frequently found in countries like Canada and USA, and start to be an attractive way of construction in many others, especially because environmental properties of wood. Contrary to other construction materials, moisture migration through a building wood-made envelope may have a significant influence on indoor air quality and air-conditioning loads, especially cooling loads [1]. Modelling of coupled heat and moisture transfer becomes hence a key point for energy performance and air quality assessment of this kind of buildings.

The phenomena of heat and mass transfer in capillary porous media have many practical applications and there is a huge amount of publications related with. For the mathematical modelling of such phenomena, either Liukov [2, 3] or de Vries [4] formulations are usually used. They are based on non-equilibrium thermodynamics and consist in a system of non-linear coupled partial differential equations which take into account the effects of the temperature gradient on the moisture migration. Non-linearity appears because the transport coefficients and the thermodynamic properties in the model are functions of either moisture content or temperature or both. A recent review of the research carried out on coupled heat and moisture transfer in building materials is provided in [5].

In spite of the existing knowledge and the amount of work carried out, building envelope models taking into account both heat and moisture transfer are rarely used in practice. The reason is the numerical added complexity compared to simple heat transfer models. For instance, simulating the thermal behaviour of the envelope of a medium-size household with a heat

conduction model involves solving a system of typically some hundreds of linear ordinary differential equations (o.d.e), while simulating its behaviour with coupled heat and moisture transfer modelling implies multiplying by two the number of o.d.e to be solved as well as moving from linear to non-linear differential equations. As a result, the simulation of the hydrothermal behaviour of buildings could be computationally intensive and damning for engineering applications, especially those requiring either a large number of simulations (i.e., sensitivity analyses, design optimization, etc.) or real-time simulations (i.e., temperature and humidity control).

While there are many situations where moisture migration through the building envelope can be neglected, modelling of coupled heat and moisture transfer becomes necessary for predicting indoor air quality and air-conditioning loads in buildings with envelopes made of wood. This paper focuses on building envelopes made of massive wood. The objective is to provide a method for accurate description of coupled heat and mass transfer phenomena within using low-dimensional models. Starting from the De Vries formulation of the problem, partial differential equations are first linearized, thus decoupled and finally reduced to a very low number of ordinary differential equations.

Section 2 describes the experimental context that has been used for models validation purposes. It includes both laboratory scale measurements of the physical properties of the studied wood as well as on-site wall monitoring. Equations governing heat transfer and moisture migration within the wall are established in Section 3, and empirical validation of the resulting model is carried out. The method proposed for linear, low-dimensional modelling of the wall behaviour is presented in Section 4. It includes both numerical and empirical validation of the results.

2. The Experimental Context

The studied wall is part of a living house built in massive wood (Figure 1, left) which is located in France (Gironde). The wall is 130mm thick, north faced. It is made up of *Pinus sylvestris* vertically glue-backed beams (Figure 1, right).

Figure 1. Picture of the building (left side) and picture of one beam (right side).

2.1. Physical properties of the wood

Main physical properties of the wood have been measured at the laboratory scale. Results achieved are briefly described here. For a detailed description of the experimental techniques that have been used and a deeper results discussion, see [6].

Sorption isotherms have been measured by the method of saturated salt solutions [7] for temperatures ranging from 20°C to 60°C. Figure 2 shows the results achieved. Points represent measurements while continuous lines come from the model:

$$w_l = \frac{w_{lm} C K \varphi}{(1 - K\varphi)(1 + CK\varphi - K\varphi)}, \tag{1}$$

where $\varphi(-)$ and w_l (kg water/kg dry matter) represent, respectively, the relative humidity and the water content at equilibrium. Parameters w_{lm}, C and K depend on both the medium nature and the temperature T(°C). Their values have been obtained by fitting model (1) to measurements (non-linear least squares method):

$$w_{lm} = -1.3786 \times 10^{-5} T^2 + 0.0004558T + 0.069,$$

$$C = 0.0064T^2 - 0.58T + 22,$$

$$K = 3.7143 \times 10^{-5} T^2 - 0.00077T + 0.747. \tag{2}$$

A very good agreement between the model and the measurements is observed. The free-water domain starts at approximately 0.12kg.kg^{-1}.

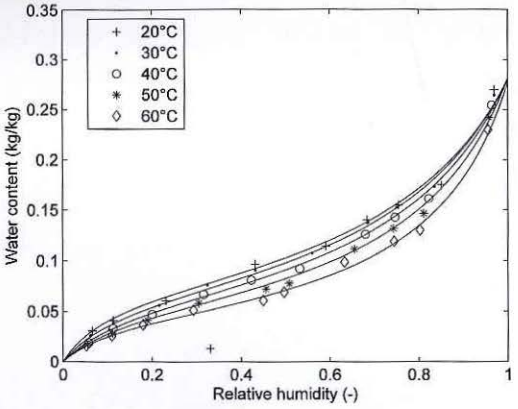

Figure 2. Sorption isotherms: measurements (symbols) and predicted values (continuous line) using model (1).

The density of dry wood has been measured on 20 different samples. Mean value retrieved is $\rho_o = 390\text{kg.m}^{-3}$, with standard deviation equal to 14kg.m^{-3}. Taking into account that the density of the cellulose is about 1200kg.m^{-3}, the porosity of dry wood is 67.5%.

The so called "hot strip method" [8] has been applied for measuring the apparent thermal conductivity (λ) and the apparent thermal effusivity (E) of the wood using 10 different samples. Results achieved for measurements carried out in the direction perpendicular to the fibres of the wood are reported in Figure 3. At $w_l = 0\text{kg.kg}^{-1}$, effusivity and conductivity values are $E = \sqrt{\rho_o c_o \lambda} = 234(\text{J.m}^{-2}.\text{K}^{-1}.\text{s}^{-1/2})$ and $\lambda = 0.11(\text{W.m}^{-1}.\text{K}^{-1})$. They allow estimating the specific heat of the dry wood: $c_o = 1276(\text{J.kg}^{-1}.\text{K}^{-1})$. We remind that apparent thermal conductivity recovers both heat conduction and heat transfer due to evaporation/condensation phenomena governed by temperature gradients (see Subsection 3.1, equation (11)).

The diffusion coefficient of water vapour within the wood when submitted to a water content gradient at uniform temperature (30°C) has been measured by a static gravimetric method [9]. Values achieved ranges from $4.9\times10^{-9}\,m^2.s^{-1}$ to $5.4\times10^{-9}\,m^2.s^{-1}$ for water contents between $0.152 kg.kg^{-1}$ and $0.164 kg.kg^{-1}$.

The permeability-to-air measurements have been carried out by the static method proposed in [10]. Values obtained range form $10^{-18}\,m^2$ to $10^{-17}\,m^2$. Consequently, we will assume in the following that heat and moisture transfers due to air flow within the wall are negligible.

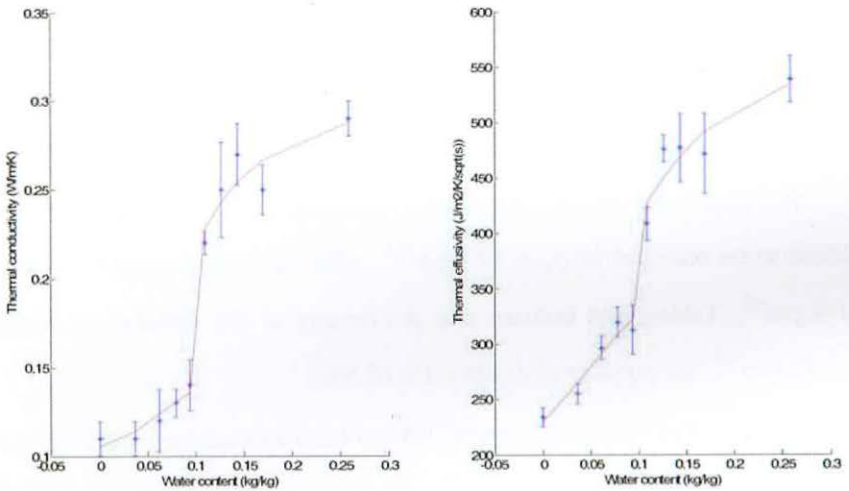

Figure 3. Apparent thermal conductivity (left side) and thermal effusivity (on the right): measurements (symbols with error bars) and simulated values (continuous line) using model (11).

2.2. On-site measurements

The thermal and humidity behaviour of the wall has been monitored from 09/27/04 to 11/10/04. Four sensors of temperature-humidity (SENSIRION SHT7x) have been placed within the wall at 20, 55, 75 and 110 mm from the indoor wall surface. Water content within the wall has been

estimated using model (1) with temperature and relative humidity recorded data. Measured time series are depicted in Figure 4 (sampling time = 10min). Figure 5 shows that the wall is working on the free-water zone ($w_l > 0.12\text{kg.kg}^{-1}$). It also evidences a low sensitivity of the water content with regard to the temperature (ranging from 10 to 25°C during the experiment).

The normalized cumulative density power spectrums (shortly cumulative spectrums or periodograms [11]) of the recorded temperature and water content data are depicted in Figure 6. We remind that this statistic describes how the variance of a time series is distributed on frequencies. When comparing the cumulative spectrums of temperature data (symbols) with the cumulative spectrums of water content (lines), it is remarked that recorded signals for water content are much richer in frequencies than temperature signals: 20% of the variance of water content signals is concentrated at frequencies beyond 24h^{-1} while only 5% of the temperature variance goes beyond; at frequencies higher than 12h^{-1}, the variance of temperature series becomes negligible while that of water content is about 5%. This is surprising because characteristics times of water diffusion are typically much lower than those of heat diffusion. As we have high confidence on temperature measurements, we conclude that measurements of water content are likely biased because the small cavities where the sensors are placed are not airtight enough. In such a case, it is expected two different vapour transfer mechanisms to be in competition. Convection due to air flow is the mechanism dominating transfers at short times (high frequencies), while diffusion dominates vapour transfer at long times (low frequencies). A deeper discussion on this point can be found in [1].

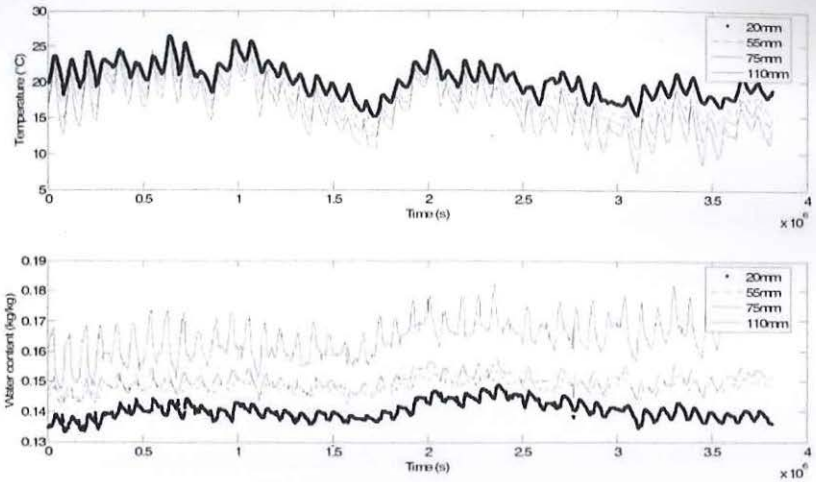

Figure 4. Measured data: temperature (top) and water content (bottom).

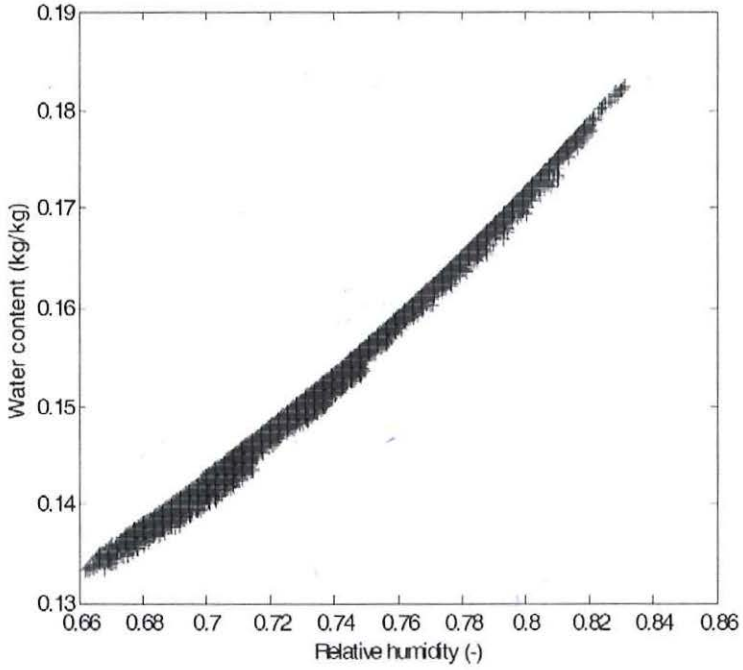

Figure 5. Water content vs. relative humidity.

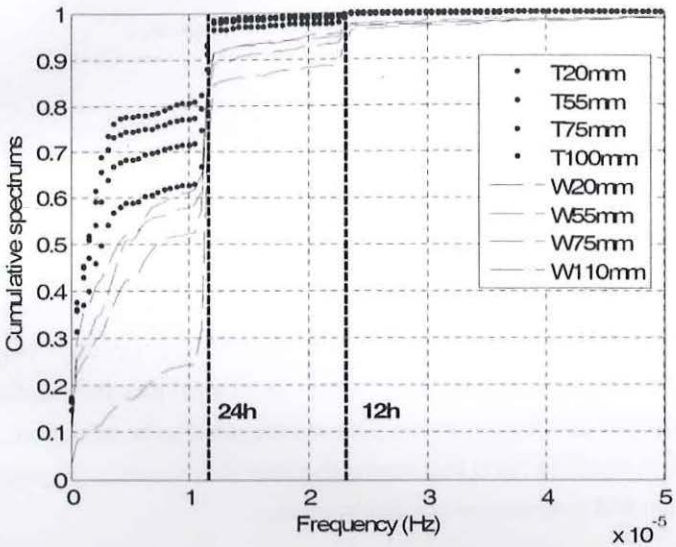

Figure 6. Cumulative spectrums for temperature time series and water content time series.

3. Heat-moisture Transfer Reference Model

Equations governing heat transfer and moisture migration within the wall are here recalled. The wall surface is assumed to be large enough compared to the thickness (L) so that 1D modelling applies. Transfer mechanisms and phenomenological laws are presented in Subsection 3.1. Next section focuses on energy and mass conservation equations. Empirical validation of the model is carried out in Subsection 3.3.

3.1. Mechanisms and phenomenology laws for transfers

Wood is a heterogeneous material made of a solid phase (wood matrix), a liquid phase (liquid water) and a gas phase (air and water vapour). At the scale of the equivalent continuum, the phenomenological laws describing mass and heat density flux can be written as:

$$J_l = -\rho_l \left(D_{wl} \frac{\partial w_l}{\partial x} + D_{Tl} \frac{\partial T}{\partial x} \right) \text{ Liquid water,} \tag{3}$$

$$J_v = -\rho_l\left(D_{wv}\frac{\partial w_l}{\partial x} + D_{Tv}\frac{\partial T}{\partial x}\right) \text{ Water vapour,} \tag{4}$$

$$J_q = -\lambda_e\frac{\partial T}{\partial x} - L_v J_v = -\lambda\frac{\partial T}{\partial x} - \rho_l L_v D_{wv}\frac{\partial w_l}{\partial x} \text{ Heat.} \tag{5}$$

T and w_l represent the temperature and the water content, respectively. ρ_l is the density of water in liquid state and L_v represents the enthalpy of water vaporisation. One must notice that equation (3) assumes that gravity and adsorption phenomena are negligible. For establishing equation (4), it is supposed that the gas within the wood works as an ideal gas. Indeed, the total pressure gradient and the air density flux are assumed to be negligible. Main assumption in equation (5) is that convective heat flux is negligible compared to conduction and evaporation-condensation flux.

Diffusion coefficients D_{wl} and D_{Tl} are generally given by:

$$D_{wl} = K_l\left(\frac{\partial \psi}{\partial w_l}\right)_T,$$

$$D_{Tl} = K_l\left(\frac{\partial \psi}{\partial T}\right)_{w_l}, \tag{6}$$

where $K_l \equiv K_l(w_l)$ is the hydraulic conductivity of the wood and ψ represents the total water potential in equilibrium with vapour (shortly water potential in the following). We remind that water potential ψ and relative humidity φ are related by the Kelvin law:

$$\varphi = \exp\left(\frac{g\psi}{R_v T}\right), \tag{7}$$

where g and R_v are, respectively, the acceleration due to gravity and the gas constant of water vapour.

As formally demonstrated in [12], diffusion coefficients D_{wv} and D_{Tv} for water vapour can be written as:

$$D_{wv} = K_v\left(\frac{\partial \psi}{\partial w_l}\right)_T,$$

$$D_{Tv} = K_v\left[\left(\frac{\partial \psi}{\partial T}\right)_{w_l} + \left(\frac{L_v - g\psi}{gT}\right)\right] \tag{8}$$

with

$$K_v = D_e \frac{P}{P - \varphi P_{vs}}\left(\frac{1}{R_v T}\right)^2 \frac{P_{vs} g\varphi}{\rho_l}, \tag{9}$$

P and P_{vs} represent the total pressure and the saturated water vapour pressure, respectively. The diffusion coefficient D_e is:

$$D_e = \varepsilon_a D_{eo} \text{ with } \varepsilon_a = 1 - \varepsilon_s - \varepsilon_l = 1 - \frac{\rho_o}{\rho_s} - \frac{\rho_o}{\rho_l} w_l, \tag{10}$$

where D_{eo} represents the diffusion of water vapour in air within the wood and ε_a is the volume fraction of gas (porosity).

As shown in equation (5), the apparent thermal conductivity of the wood is defined as:

$$\lambda = \lambda_e + \rho_l L_v D_{Tv} \tag{11}$$

λ_e is the so called effective thermal conductivity, which is generally assumed to be dependent on moisture content as follows:

$$\lambda_e = \lambda_{sa} + \lambda_{la} w_l, \tag{12}$$

where λ_{sa} and λ_{la} represent, respectively, the thermal conductivity of dry wood and the sensitivity to the moisture content. Model (11) with equations (8), (9) and (12) has been fitted on the available data for apparent thermal conductivity in order to estimate values of parameters λ_{sa}, λ_{la} and D_{eo}. Results achieved are reported in Table 1. As shown in Figure 3, there is a quite good agreement between model (11) and measurements.

Table 1. Parameters of model (11): values obtained by fitting the model on measured data of apparent thermal conductivity

	$w_l \leq 0.12\text{kg.kg}^{-1}$	$w_l > 0.12\text{kg.kg}^{-1}$
$\lambda_{sa}(\text{W.m}^{-1}.\text{K}^{-1})$	0.1053	0.1298
$\lambda_{la}(\text{W.m}^{-1}.\text{K}^{-1})$	0 (freezed)	0.0084
$D_{eo}(\text{m}^2.\text{s}^{-1})$	3.905×10^{-5}	1.046×10^{-4}

3.2. Energy and mass conservation equations

One-dimensional mass and energy conservation equations can be written as:

$$\rho_o \frac{\partial}{\partial t}(w_l + w_v) = -\frac{\partial}{\partial x}(\vec{J}_l + \vec{J}_v), \tag{13}$$

$$\rho_o \frac{\partial}{\partial t}(h_s + w_l h_l + w_v h_v) = -\frac{\partial}{\partial x}\vec{J}_q, \tag{14}$$

ρ_o is the density of dry wood and w_v represents the water vapour content. The enthalpies of the phases are:

$$h_s = c_s(T - T_{ref}), \quad h_l = c_l(T - T_{ref}), \quad h_v = c_v(T - T_{ref}) + L_v, \tag{15}$$

where c_s, c_l and c_v are the corresponding specific heats. Dimensionless analyses carried out in [13] prove that the effect of w_v in the left part of equations (4) and (5) can be neglected. It is also shown that $\vec{J}_l << \vec{J}_v$ under actual wall working conditions. Hence, reporting equations (4)-(5) and equation (15) into equations (13)-(14) yields equations $(0 < x < L)$:

$$\rho_o c \frac{\partial T(x,t)}{\partial t} = \frac{\partial}{\partial x}\left(\lambda_e \frac{\partial T(x,t)}{\partial x}\right) + \rho_o L_v \frac{\partial w_l(x,t)}{\partial t},$$

$$\rho_o \frac{\partial w_l(x,t)}{\partial t} = \frac{\partial}{\partial x}\left(\rho_l D_{Tv} \frac{\partial T(x,t)}{\partial x}\right) + \frac{\partial}{\partial x}\left(\rho_l D_{wv} \frac{\partial w_l(x,t)}{\partial x}\right). \tag{16}$$

They can also be written as:

$$\rho_o c \frac{\partial T(x,t)}{\partial t} = \frac{\partial}{\partial x}\left(\lambda \frac{\partial T(x,t)}{\partial x}\right) + \frac{\partial}{\partial x}\left(\rho_l L_v D_{wv} \frac{\partial w_l(x,t)}{\partial x}\right),$$

$$\rho_o \frac{\partial w_l(x,t)}{\partial t} = \frac{\partial}{\partial x}\left(\rho_l D_{Tv} \frac{\partial T(x,t)}{\partial x}\right) + \frac{\partial}{\partial x}\left(\rho_l D_{wv} \frac{\partial w_l(x,t)}{\partial x}\right), \qquad (17)$$

c represents the apparent specific heat. It is given by:

$$c = c_s + c_l w_l + c_v w_v \text{ with } w_v = \frac{\varepsilon_a \rho_v}{\rho_o} = \frac{\varepsilon_a}{\rho_o} \frac{\varphi P_{vs}}{R_v T}. \qquad (18)$$

Boundary conditions of first kind are considered:

$$\begin{cases} T(0,t) = T_{x=0}(t) & w_l(0,t) = w_{l_{x=0}}(t), \\ T(L,t) = T_{x=L}(t) & w_l(L,t) = w_{l_{x=L}}(t). \end{cases} \qquad (19)$$

3.3. Empirical validation

Validation of the model given by equations (17) and (19) is carried out by comparing temperature and water content measurements to simulations. Taking into account available on-site measurements, a wall of 90mm in thickness instead of 130mm has been considered. Prescribed temperature and water content at the boundaries of the modeled wall are hence assumed to be given by the measured data at 20mm and 110mm from the indoor surface of the actual wall. Observations for model/data comparisons are temperature and water content values at 55mm and 75mm from the indoor surface of the actual wall. They are referred as $(T_{55\text{mm}}, w_{l_{55\text{mm}}})$ and $(T_{75\text{mm}}, w_{l_{75\text{mm}}})$ in the following.

Sorption isotherms are calculated using equations (1)-(2). Water vapor diffusion coefficients are given by equations (8)-(9). Model (12)-(13) is used for calculating apparent thermal conductivity while equation (18) supplies apparent specific heat values. Measured/estimated values of ρ_o, c_o and D_{eo}

have been used: $\rho_o = 390\text{kg.m}^{-3}$, $c_o = 1276\text{J.kg}^{-1}\text{.K}^{-1}$ and $D_{eo} = 1.046 \times 10^{-4}\text{m}^2\text{.s}^{-1}$. Besides, we remind that $P = 101325\text{Pa}$, $R_v = 461.52\text{J.kg}^{-1}\text{.K}^{-1}$, $g = 9.81\text{m.s}^{-2}$, $\rho_s = 1200\text{kg.m}^{-3}$, $\rho_l = 1000\text{kg.m}^{-3}$, $c_l = 4181\text{J.kg}^{-1}\text{.K}^{-1}$, $c_v = 1868\text{J.kg}^{-1}\text{.K}^{-1}$ and $L_v = 2440000\text{J.kg}^{-1}$.

The method of finite volumes has been used for spatial discretization of equations (17) and (19). This leads to the following non-linear, $2n$-dimensional $(n = 130)$ state model:

$$\frac{d}{dt}\begin{bmatrix}\mathbf{T}(t)\\ \mathbf{w}(t)\end{bmatrix} = \mathbf{A}\begin{bmatrix}\mathbf{T}(t)\\ \mathbf{w}(t)\end{bmatrix} + \mathbf{E}\begin{bmatrix}T_{x=0}(t)\\ w_{lx=0}(t)\\ T_{x=L}(t)\\ w_{lx=L}(t)\end{bmatrix} \tag{20}$$

$\mathbf{T}(t)$ is the vector $(n \times 1)$ of temperatures at the control volumes while $\mathbf{w}(t)$ is the vector $(n \times 1)$ of water contents. The elements of matrices $\mathbf{A}$ $(2n \times 2n)$ and $\mathbf{E}$ $(2n \times 4)$ depend on both the temperature and the water content.

Time-integration of the state model above has been carried out using the modified Rosenbrock method [14] implemented in the "ode15s" function of Matlab. Measured temperatures $T_{55\text{mm}}$ and $T_{75\text{mm}}$ (symbols) as well as simulated ones (continuous lines) are depicted at the top side of Figure 7, while the simulation error is represented at the bottom. A very good agreement is observed between measurements and simulations. It can be seen that differences between measurements and simulations are most of the time within the interval of measurements uncertainty (±0.5°C).

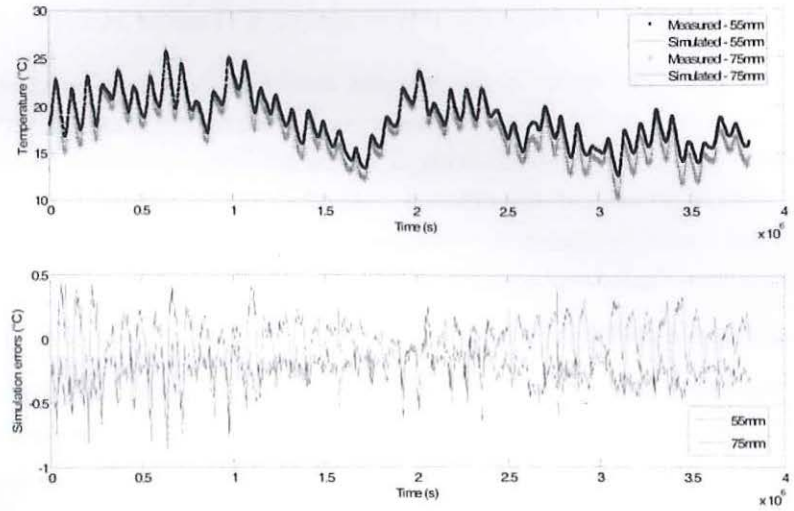

Figure 7. Comparison between temperature measurements and simulations: temperature time series (top) and simulation errors (bottom).

As expected, a significant disagreement is observed between $w_{55\text{mm}}$ and $w_{75\text{mm}}$ measured values and simulations (Figure 8). However, because of unreliability of water content measurements (see Subsection 2.2) such results cannot be used for model rejection. From a physical point of view, model simulations behave better than measurements because smoother. Indeed, the model is able to describe main trends (low-frequency behaviour) observed in the data. The differences between measurements and simulation are always less than 6%.

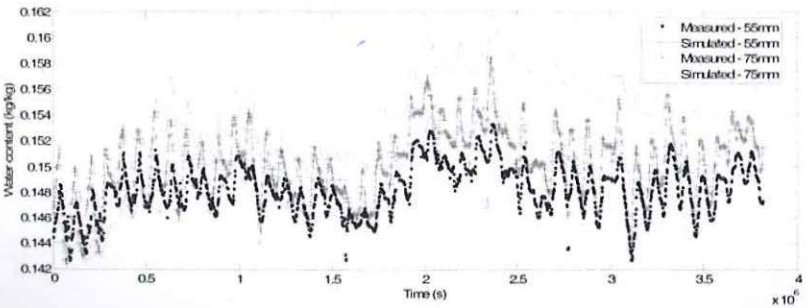

Figure 8. Comparison between water content measurements and simulations.

4. Linear, Low-dimensional Heat-moisture Transfer Model

The non-linear model in the previous section is here considered as a reference model. In Subsection 4.1, we prove that the reference model can be replaced by a linearized model without significant loss of accuracy. In next two sections a method for efficient reduction of the dimension of the linearized model is described. Subsection 4.4 focuses on validation of the resulting low-dimensional approximation of the studied problem.

4.1. Reference model linearization

Non-linear nature of the reference model is due to the variations of coefficients λ, c, D_{Tv} and D_{wv} with the temperature and the water content. Using the values of temperature and water content within the wall that have been simulated with the reference model, coefficients λ, c, D_{Tv} and D_{wv} have been calculated. Results achieved are depicted in Figure 9. The apparent specific heat only depend on the water content, while coefficients λ, D_{Tv} and D_{wv} depend on both temperature and water content. However, under actual wall working conditions, variations of λ, D_{Tv} and D_{wv} with water content are not really significant (see Figure 9, low dispersion of points around the trend).

A linear version of the reference model (linearized model in the following) can be reached by freezing λ, c, D_{Tv} and D_{wv} coefficients to suitable constant values. An efficient iterative method for automatic linearization of non-linear diffusion models has been proposed in [15]. It is proven that the 'best' linear approximate model is obtained when replacing non-linear parameters by their respective mean values. Taking inspiration on this previous work, constant values for coefficients λ, c, D_{Tv} and D_{wv} have been calculated as follows:

$$\theta = \int_{t=0}^{t_{end}} \int_{x=0}^{L} \theta(T(x,t),\, w_l(x,t))\, dx dt, \quad \theta = \lambda,\, c,\, D_{Tv},\, D_{wv}, \qquad (21)$$

where $T(x, t)$ and $w_l(x, t)$ represent the temperature field and the water

content field simulated with the reference model. This leads to $\lambda = 0.2452 \text{W.m}^{-1}.\text{K}^{-1}$, $c = 1906.7 \text{J.kg}^{-1}.\text{K}^{-1}$, $D_{Tv} = 4.7082 \times 10^{-11} \text{m}^2.\text{s}^{-1}.\text{K}^{-1}$ and $D_{wv} = 4.9754 \times 10^{-9} \text{m}^2.\text{s}^{-1}$.

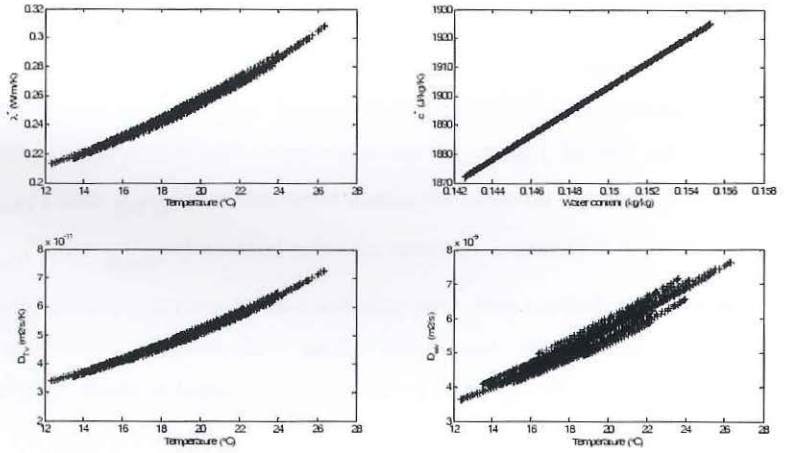

Figure 9. Variation of reference model coefficients λ, c, D_{Tv} and D_{wv} with the temperature and the water content.

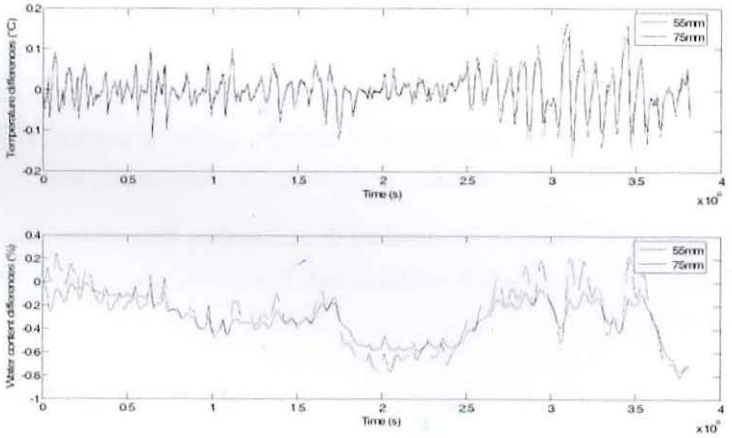

Figure 10. Comparison between the reference and the linearized models. Differences in terms of simulated temperatures (top) and simulated water contents (bottom).

The linearized model is hence defined by equations (17) and (19) with the values above for λ, c, D_{Tv} and D_{wv} coefficients. As previously, the finite volumes method has been used for spatial discretization of the linearized model. This yields a $2n$-dimensional $(n = 260)$ state model as the one given by equation (20) but with constant **A** and **E** matrices. The modified Rosenbrock method has been used again for time-integration of the state model. Simulation results have been compared with those of the reference model. At the top of Figure 10 are represented the differences observed between both model in terms of simulated temperatures ($T_{55\text{mm}}$ and $T_{75\text{mm}}$), while the relative differences in terms of water content ($w_{l_{55\text{mm}}}$ and $T_{l_{75\text{mm}}}$) are depicted at the bottom part. One remarks a quite good agreement between both models. This proves that, under actual wall working conditions, the reference model can be replaced by a linearized model without significant loss of accuracy.

4.2. Decoupling heat and moisture equations

As evidence in recent reviews [16, 17], there is numerous and efficient techniques that can be used to reduce the dimension of linear time-invariant state models. They could be directly applied to the state model associated to the linearized heat-moisture transfer problem (equation (20) with constant matrices). However, as shown in next section, higher numerical efficiency will be achieved if heat and moisture equations are first decoupled.

Firstly, let us consider the standard dimensionless form of such equations (equation (16) with constant coefficients). For points within the wall, they are written as:

$$\frac{\partial \theta_1(\bar{x}, \tau)}{\partial \tau} = \frac{\partial^2 \theta_1(\bar{x}, \tau)}{\partial \bar{x}^2} - Ko \frac{\partial \theta_2(\bar{x}, \tau)}{\partial \tau},$$

$$\frac{\partial \theta_2(\bar{x}, \tau)}{\partial \tau} = Lu \frac{\partial^2 \theta_2(\bar{x}, \tau)}{\partial \bar{x}^2} - LuPn \frac{\partial^2 \theta_1(\bar{x}, \tau)}{\partial \bar{x}^2} \qquad (22)$$

with:

$$\theta_1 = \frac{T - T_o}{T_s - T_o} \text{ (dimensionless temperature);}$$

$$\theta_2 = \frac{w_{l_o} - w_l}{w_{l_o} - w_{l_s}} \text{ (dimensionless moisture);}$$

$$Ko = \frac{L_v}{c} \frac{w_{l_o} - w_{l_s}}{T_s - T_o} \text{ (Kossovitch number);}$$

$$Lu = \frac{\alpha_m}{\alpha} \text{ (Luikov number);}$$

$$Pn = \delta \frac{T_s - T_o}{w_{l_o} - w_{l_s}} \text{ (Possnov number);}$$

$$\tau = \frac{\alpha t}{L^2} \text{ (dimensionless time);}$$

$$\bar{x} = \frac{x}{L} \text{ (dimensionless coordinate)}$$

(T_o, w_{l_o}) and (T_s, w_{l_s}) represent constant temperature and moisture values chosen for dimensionless variables definition. $\alpha = \lambda_e/\rho_o c$ is the effective thermal diffusivity and $\alpha_m = \rho_l D_{Tv}/\rho_o c$ is the diffusion coefficient of moisture. $\delta = D_{Tv}/D_{wv}$ represents the so called thermogradient coefficient.

Boundary conditions (equation (19)) become:

$$\begin{cases} \theta_1(0, \tau) = \theta_{1,\bar{x}=0}(\tau) & \theta_2(0, \tau) = \theta_{2,\bar{x}=0}(\tau), \\ \theta_1(1, \tau) = \theta_{1,\bar{x}=1}(\tau) & \theta_2(1, \tau) = \theta_{2,\bar{x}=1}(\tau) \end{cases} \tag{23}$$

with $\theta_{1,\bar{x}} = (T_x - T_o)/(T_s - T_o)$ and $\theta_{2,\bar{x}} = (w_{l_o} - w_{l,x})/(w_{l_o} - w_{l_s})$.

It is well known that the coupled system of partial differential equations (22) can be reduced to decoupled pure heat conduction equations where the

potentials are presented by combined variables being a linear combination of output variables [18]. The transformation from the potentials $\theta_{k=1,2}(\bar{x}, \tau)$ to new functions $Z_{k=1,2}(\bar{x}, \tau)$, is taken as (see, i.e., [19] for derivation):

$$Z_k(\bar{x}, \tau) = \theta_1(\bar{x}, \tau) + \frac{\nu_k^2 - 1}{Pn}\theta_2(\bar{x}, \tau), \quad (k = 1, 2), \tag{24}$$

where

$$\nu_k^2 = \frac{1}{2}\left\{\left(1 + KoPn + \frac{1}{Lu}\right) + (-1)^k\sqrt{\left(1 + KoPn + \frac{1}{Lu}\right)^2 - \frac{4}{Lu}}\right\} (k = 1, 2). \tag{25}$$

Thus, from equation (24) it follows

$$\theta_1(\bar{x}, \tau) = \frac{1}{\nu_2^2 - \nu_1^2}[(\nu_2^2 - 1)Z_1(\bar{x}, \tau) - (\nu_1^2 - 1)Z_2(\bar{x}, \tau)],$$

$$\theta_2(\bar{x}, \tau) = \frac{Pn}{\nu_2^2 - \nu_1^2}[Z_2(\bar{x}, \tau) - Z_1(\bar{x}, \tau)] \tag{26}$$

and from equation (25)

$$\nu_1^2\nu_2^2 = \frac{1}{Lu} \text{ and } (\nu_1^2 - 1)(\nu_2^2 - 1) = -KoPn. \tag{27}$$

Introducing equation (25) into problem (22)-(23) and using the relations (27), the system of equations governing the evolution of the functions $Z_{k=1,2}(\bar{x}, \tau)$ becomes:

$$\nu_k^2 \frac{\partial Z_k(\bar{x}, \tau)}{\partial \tau} = \frac{\partial^2 Z_k(\bar{x}, \tau)}{\partial \bar{x}^2} \quad (k = 1, 2) \tag{28}$$

subject to the boundary conditions given by:

$$Z_k(0, \tau) = \theta_1(0, \tau) + \frac{\nu_k^2 - 1}{Pn}\theta_2(0, \tau), \quad (k = 1, 2),$$

$$Z_k(1, \tau) = \theta_1(1, \tau) + \frac{\nu_k^2 - 1}{Pn}\theta_2(1, \tau), \quad (k = 1, 2). \tag{29}$$

Hence, the solution of the linearized problem of heat and moisture transfer within the wood can be obtained by solving two decoupled diffusion equations.

4.3. Model size reduction

The so called truncation methods are the most widely used techniques for linear, time-invariant state models reduction. They are based on the use of proper (often orthogonal) basis allowing identification of some few dominant components (referred as directions, eigenvectors or modes), so that a low-dimensional approximate description of the problem is obtained by projection of the initial high-dimensional model on the dominant eigenvectors of the basis.

Let us consider the two models given by equations (28) and (29). After convenient spatial discretization, the two following n-dimensional state models $(k = 1, 2)$ are obtained:

$$\nu_k^2 \frac{d\mathbf{Z}_k(t)}{dt} = \mathbf{M}\mathbf{Z}_k(t) + \mathbf{N}\mathbf{U}_k(t) \tag{30}$$

$\mathbf{Z}_k(t)$ is the vector $(n \times 1)$ of $Z_k(\bar{x}, \tau)$ values at the control volumes, while $\mathbf{U}_k(t) = [Z_k(0, \tau)\ Z_k(1, \tau)]^t$. Dimensions of matrices $\mathbf{M}$ and $\mathbf{N}$ are $(n \times n)$ and $(n \times 2)$, respectively. In matrix form, dimensionless temperature and water content within the wall are written as:

$$\boldsymbol{\theta}(t) = \mathbf{H}\mathbf{Z}(t) \tag{31}$$

with

$$\boldsymbol{\theta}(t) = \begin{bmatrix} \boldsymbol{\theta}_1(t) \\ \boldsymbol{\theta}_2(t) \end{bmatrix};\ \mathbf{Z}(t) = \begin{bmatrix} \mathbf{Z}_1(t) \\ \mathbf{Z}_2(t) \end{bmatrix};\ \mathbf{H} = \frac{1}{\nu_2^2 - \nu_1^2} \begin{bmatrix} 2(\nu_2^2 - 1)\mathbf{I} & 2(\nu_1^2 - 1)\mathbf{I} \\ -Pn\mathbf{I} & Pn\mathbf{I} \end{bmatrix}.$$

The objective of model reduction is to replace equations (30)-(31) by a lower size $(2r << 2n)$ state model of the general form:

$$\begin{cases} \dfrac{d\mathbf{X}_k(t)}{dt} = \mathbf{F}_k\mathbf{X}_k(t) + \mathbf{B}_k\mathbf{U}_k(t), \\ \tilde{\boldsymbol{\theta}}(t) = \mathbf{C}\mathbf{X}(t) + \mathbf{D}\mathbf{U}(t) \end{cases} \tag{32}$$

so that $\widetilde{\boldsymbol{\theta}}(t)$ provides an accurate enough approximation of $\boldsymbol{\theta}(t)$. Dimensions of vector and matrices in equation above are now: $\mathbf{X}_k(t)(r \times 1)$, $\mathbf{F}_k(r \times r)$, $\mathbf{B}_k(r \times 2)$ and $\mathbf{C}(n \times r)$. Besides, $\mathbf{X}(t) = [\mathbf{X}_1(t)\ \mathbf{X}_2(t)]^t$ and $\mathbf{U}(t) = [\mathbf{U}_1(t)\ \mathbf{U}_2(t)]^t$.

First step of model reduction consists in rewriting equations (30)-(31) by considering $\mathbf{Z}_k(t) = \mathbf{Z}_k^s(t) + \mathbf{Z}_k^d(t)$, where the so called pseudo static regime is defined by:

$$\mathbf{0} = \mathbf{M}\mathbf{Z}_k^s(t) + \mathbf{N}\mathbf{U}_k(t) \Rightarrow \mathbf{Z}_k^s(t) = -\mathbf{M}^{-1}\mathbf{N}\mathbf{U}_k(t). \tag{33}$$

Doing so, it can be easily proven that equations (30)-(31) become:

$$\begin{cases} \dfrac{d\mathbf{Z}_k^d(t)}{dt} = \mathbf{M}_k\mathbf{Z}_k^d(t) + \mathbf{N}_k\dfrac{d\mathbf{U}_k(t)}{dt}, \\ \boldsymbol{\theta}(t) = \mathbf{H}\mathbf{Z}^d(t) + \mathbf{S}\mathbf{U}(t) \end{cases} \tag{34}$$

with

$$\mathbf{M}_k = (1/\nu_k^2)\mathbf{M};\ \ \mathbf{N}_1 = \mathbf{N}_2 = \mathbf{M}^{-1}\mathbf{N};\ \ \mathbf{S} = -\mathbf{H}[\mathbf{N}_1\ \mathbf{N}_2]. \tag{35}$$

As explained in [20], moving from equation (32) to equation (34) has the advantage of allowing model reduction without perturbation of the static behaviour of the system. Reduction is applied so that $\mathbf{Z}_k^s(t)$ remains unchanged, only $\mathbf{Z}_k^d(t)$ will be approached.

Second step of model reduction is a fundamental step. The objective is to choose and to calculate a suitable projection basis, also called *transformation matrix* $\mathbf{P}_k(n \times n)$. The choice of the basis makes the main difference among reduction methods [16]. The most popular one in thermal analysis is the modal basis (i.e., [20]), which comes from spectral decomposition of the state matrix $\mathbf{M}_k$. On the contrary, people working in control prefer using the so called balanced realisation [21]. Most striking feature of reduction

methods based on balanced realisation is accuracy. They provide optimal approximations of the initial model in the sense of different useful norms of the approximation error. Counterpart is the computing time required for calculating them, which is much more important that the time required by modal approximations. An attractive balance between accuracy and computing time is provided by the so called singular basis recently proposed by Ait-Yahia and Palomo del Barrio [22, 23]. It takes inspiration of Singular Values Decomposition techniques and provides nearly optimal approximations of the initial model with computing times comparable to that of modal approaches. It is the one chosen in this paper and briefly described below.

Calculating the singular basis $\mathbf{P}_k$ involves first computing the controllability gramien $\mathbf{W}_k(n \times n)$ of system (34) by solving the following Lyapunov equation:

$$\mathbf{M}_k\mathbf{W}_k + \mathbf{M}_k^t\mathbf{W}_k + \mathbf{N}_k\mathbf{N}_k^t = \mathbf{0}. \tag{36}$$

Thus, carrying out spectral decomposition of $\mathbf{W}_k$. As $\mathbf{W}_k$ is a symmetric, positive definite matrix, this yields

$$\mathbf{W}_k = \mathbf{P}_k\mathbf{\Sigma}_k\mathbf{P}_k^t \tag{37}$$

$\mathbf{\Sigma}_k = diag[\sigma_{1,k}^2\ \sigma_{2,k}^2 \cdots \sigma_{n,k}^2]$ with $\sigma_{1,k}^2 \geq \sigma_{2,k}^2 \geq \cdots \geq \sigma_{n,k}^2 > 0$ is a diagonal matrix including $\mathbf{W}_k$ eigenvalues($\mathbf{W}_k$ eigenvectors are column-wise placed in $\mathbf{P}_k$. They form an orthogonal basis: $\mathbf{P}_k^t\mathbf{P}_k = \mathbf{I}$.

According to equation (35), Lyapunov equations above $(k = 1, 2)$ can also be written as:

$$\left.\begin{aligned}\mathbf{M}\mathbf{W}_1 + \mathbf{M}^t\mathbf{W}_1 + \nu_1^2\mathbf{N}_o\mathbf{N}_o^t = \mathbf{0}\\ \mathbf{M}\mathbf{W}_2 + \mathbf{M}^t\mathbf{W}_2 + \nu_2^2\mathbf{N}_o\mathbf{N}_o^t = \mathbf{0}\end{aligned}\right\} \Rightarrow \begin{aligned}\nu_2^2\mathbf{M}\mathbf{W}_1 + \nu_2^2\mathbf{M}^t\mathbf{W}_1 + \nu_2^2\nu_1^2\mathbf{N}_o\mathbf{N}_o^t = \mathbf{0}\\ \nu_1^2\mathbf{M}\mathbf{W}_2 + \nu_1^2\mathbf{M}^t\mathbf{W}_2 + \nu_1^2\nu_2^2\mathbf{N}_o\mathbf{N}_o^t = \mathbf{0}\end{aligned} \tag{38}$$

with $\mathbf{N}_o = \mathbf{N}_1 = \mathbf{N}_2$. This means that $v_2^2\mathbf{W}_1 = v_1^2\mathbf{W}_2$ and consequently $\mathbf{P} = \mathbf{P}_1 = \mathbf{P}_2$. This is an important result that highlights the interest of decoupling heat and moisture equations as done in Subsection 4.3. In practice, getting $\mathbf{P} = \mathbf{P}_1 = \mathbf{P}_2$ involves solving one Lyapunov equation of dimension $(n \times n)$ instead of $(2n \times 2n)$, thus diagonalization of an $(n \times n)$-matrix instead of a $(2n \times 2n)$-matrix. For small problems (say less than 500 ode), it is recommended to apply standard methods (i.e., Bartels-Stewart [24] and Hammarling [25]) to solve the Lyapunov equation. Large sparse Lyapunov equations, as those coming from heat transfer problems, can be efficiently solved by iterative Krylov subspace methods [26].

Third step of model reduction involves projection of model (34) on the dominant eigenvectors of $\mathbf{P}$, which are those associated to the largest eigenvalues. Let $\mathbf{P}_r$ be the matrix including the first r columns of $\mathbf{P}$. A $2r$-dimensional approximation of the studied problem is achieved by applying the transformations $\mathbf{Z}_1^d(t) = \mathbf{P}_r\overline{\mathbf{Z}}_1(t)$ and $\mathbf{Z}_2^d(t) = \mathbf{P}_r\overline{\mathbf{Z}}_2(t)$ to equation (34). Taking into account that $\mathbf{P}_r^t\mathbf{P}_r = \mathbf{I}$, this leads to:

$$\begin{cases} \dfrac{d\overline{\mathbf{Z}}_k(t)}{dt} = \overline{\mathbf{M}}_k\overline{\mathbf{Z}}_k(t) + \overline{\mathbf{N}}_o\dfrac{d\mathbf{U}_k(t)}{dt}, \\ \widetilde{\boldsymbol{\theta}}(t) = \overline{\mathbf{H}}\overline{\mathbf{Z}}(t) + \mathbf{S}\mathbf{U}(t) \end{cases} \tag{39}$$

with $\overline{\mathbf{M}}_k = \mathbf{P}_r^t\mathbf{M}_k\mathbf{P}_r (r \times r)$, $\overline{\mathbf{N}}_o = \mathbf{P}_r^t\mathbf{N}_o (r \times 2)$ and $\overline{\mathbf{H}} = \mathbf{H}\begin{bmatrix}\mathbf{P}_r \\ \mathbf{P}_r\end{bmatrix}(2n \times 2r)$.

To avoid $\mathbf{U}$ time-derivatives in equation above, the following change of variables can be applied: $\overline{\mathbf{Z}}_k(t) \leftarrow \overline{\mathbf{Z}}_r(t) - \mathbf{N}_o\mathbf{U}_k(t)$. We get:

$$\begin{cases} \dfrac{d\overline{\mathbf{Z}}_k(t)}{dt} = \overline{\mathbf{M}}_k\overline{\mathbf{Z}}_k(t) + \overline{\mathbf{N}}_o\mathbf{U}_k(t), \\ \widetilde{\boldsymbol{\theta}}(t) = \overline{\mathbf{H}}\overline{\mathbf{Z}}(t) + \mathbf{S}\mathbf{U}(t) \end{cases} \tag{40}$$

with $\overline{\mathbf{N}}_o \leftarrow \overline{\mathbf{M}}_k\overline{\mathbf{N}}_o$ and $\mathbf{S} \leftarrow \mathbf{S} + \overline{\mathbf{H}}\begin{bmatrix}\mathbf{N}_o \\ \mathbf{N}_o\end{bmatrix}$.

4.4. Validation

The reduction technique described above has been applied for reaching low-dimensional approximations of the linearized problem of heat-moisture transfer within the wood. We remind that coefficients of the linearized model are $\delta = 0.0127$, $\alpha = 1.7518 \times 10^{-7}\,\mathrm{m}^2.\mathrm{s}^{-1}$ and $\alpha_m = 9.5075 \times 10^{-9}\,\mathrm{m}^2.\mathrm{s}^{-1}$. $(T_o,\, w_{l_o})$ and $(T_s,\, w_{l_s})$ values for dimensionless variables definition are $(7.3\,^{\circ}\mathrm{C},\, 0.1332\,\mathrm{kg/kg})$ and $(26.6\,^{\circ}\mathrm{C},\, 0.1824\,\mathrm{kg/kg})$, respectively. This leads to $Lu = 0.0543$, $Ko = 3.2686$ and $Pn = 4.9713$.

Reduced models of dimension up to 10 have been calculated and used for simulating the wall behaviour. The relative approximation errors associated to these models are defined as:

$$e_T(x,\, t) = \left| \frac{T(x,\, t) - \widetilde{T}(x,\, t)}{T(x,\, t)} \right| \times 100,$$

$$e_w(x,\, t) = \left| \frac{w_l(x,\, t) - \widetilde{w}_l(x,\, t)}{w_l(x,\, t)} \right| \times 100,$$

where $T(x,\, t)$ and $w_l(x,\, t)$ represent, respectively, the field of temperature and water content field predicted by the full-dimension $(2n = 260)$ model, while $\widetilde{T}(x,\, t)$ and $\widetilde{w}_l(x,\, t)$ are those retrieved by using low-dimension models $(2r = 4,\, 6,\, 8,\, 10)$. The maximum values

$$e_{T,\max} = \max_{0<x<L,\, 0<t<t_{end}} [e_T(x,\, t)],$$

$$e_{w_l,\max} = \max_{0<x<L,\, 0<t<t_{end}} [e_{w_l}(x,\, t)]$$

provide a first evaluation of the reduced models. Table 2 shows that both $e_{T,\max}$ and $e_{w_l,\max}$ decrease when increasing the model dimension as expected. Besides, it can be seen that maximum relative error associated to the 4-dimension model are already very low.

Table 2. Evaluation of the low-dimension models through the associated maximum value of the relative approximation error in predicted temperatures and water contents

Model dimension $2r$	$e_{T,\max}(\%)$	$e_{w_l,\max}(\%)$
4	0.0576	0.1730
6	0.0069	0.0328
8	0.0042	0.0186
10	0.0019	0.0089

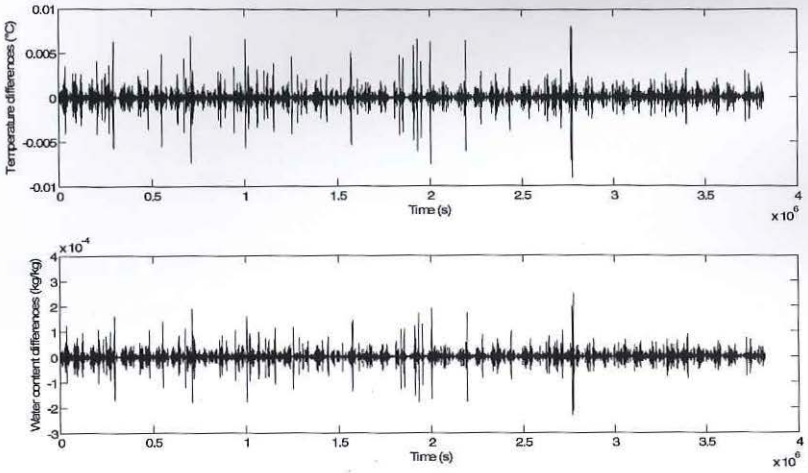

Figure 11. Comparison between the full-dimension model and the reduced 4-dimension model. Differences in terms of simulated temperatures (top) and simulated water contents (bottom).

Figures 11 to 13 allow a better appreciation of the quality of the 4-dimensional model (4 ode). In Figures 11 and 12, it is compared with the full-dimension model (260 ode), while in Figure 13, it is compared with temperature measurements.

At the top of Figure 11 are represented the differences $T(x, t) - \widetilde{T}(x, t)$, while $w_l(x, t) - \widetilde{w}_l(x, t)$ approximation errors are depicted at the bottom. There are as many curves as control volumes in the discretized linearized model (130). An excellent agreement is observed between the full-dimension and the 4-dimension models. Heat flux and water vapour flux at the wall boundaries predicted by the full-dimension model (symbols) and the 4-dimension model (continuous lines) are depicted in Figure 12. Again, the agreement between both models is excellent.

Figure 13 shows the differences observed between the available temperature data (measurements at 55mm and 75mm from the indoor surface of the actual wall) and the 4-dimension model predictions. Comparing such results with those in Figure 7, we can conclude that no significant differences exist between the linear 4-dimension model and the non-linear 260-dimension model. On the contrary, using the 4-dimension model allows reducing more than 99.9% the CPU time required for simulating the wall behaviour.

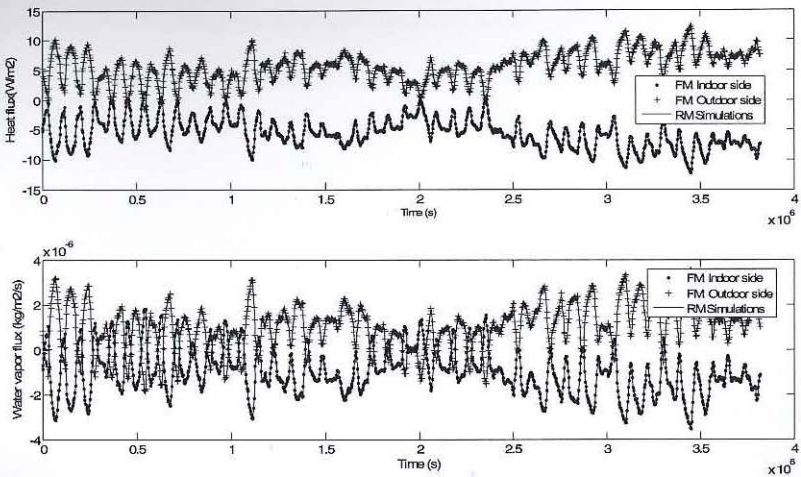

Figure 12. Comparison between the full-dimension model (FM, symbols) and the reduced 4-dimension model (RM, continuous lines). Heat flux (top) and water vapor flux (bottom) at the wall boundaries.

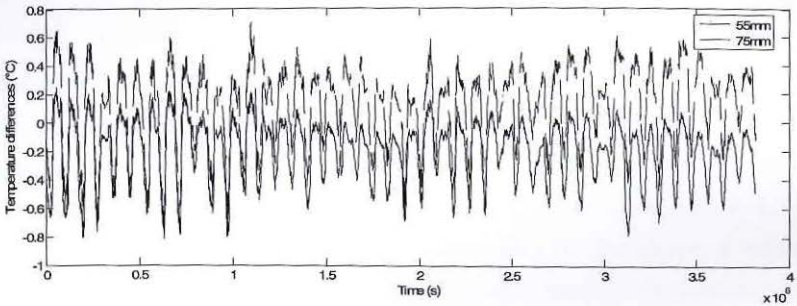

Figure 13. Difference between the temperatures predicted by the reduced 4-dimension model and the measurements.

5. Conclusion

A method for accurate description of coupled heat and mass transfer phenomena within wood-walls using linear, low-dimensional models has been proposed. Starting from De Vries formulation of the problem, partial differential equations are first linearized, thus decoupled and finally reduced to a very low number of ordinary differential equations using a powerful method based on singular valued decomposition techniques.

Progressive empirical and numerical validation of the results has been carried out. First validation (empirical) refers to the non-linear full-dimensional model. The second one (numerical) shows that such model can be replaced by a linearized model without significant loss of accuracy. Last one (numerical and empirical) proves that a simple linear, time-invariant state model form by 4 ordinary differential equations is able to provide excellent results when it is used to predict temperature and water content behavior of the studied wall. A very significant reduction of the CPU time is achieved using this model instead of the initial, high-dimensional one.

Acknowledgement

The authors acknowledge the financial support of the French Research National Agency for subsidizing DYNASIMUL and SIMINTHEC Projects.

References

[1] N. Mendes, F. C. Winkelmann, R. Lamberts and P. C. Philippi, Moisture effects on conduction loads, Energy and Buildings 35 (2003), 631-644.

[2] A. V. Liukov, System of differential equations of heat and mass transfer in capillary porous bodies, Int. J. Heat Mass Transfer 18 (1975), 1-14.

[3] A. V. Liukov, Heat and Mass Transfer, Mir, Moscow, 1980.

[4] D. A. de Vries, Simultaneous transfer of heat and moisture in porous media, Trans. Am. Geophys. Union 39 (1958), 909-916.

[5] M. Qin, R. Belarbi, A. Aït-Mokhtar and L. O. Nilsson, Coupled heat and moisture transfer in multi-layer building materials, Construction and Building Materials 23 (2009), 967-975.

[6] S. Raji, Caractérisation hygro thermique, par une approche multi échelle, de constructions en bois massif en vue d'amélioration énergétique et de valorization environnementale, PhD, Université Bordeaux 1, 2006.

[7] A. Talla, Y. Jannot, G. Nkeng and J. R. Puiggali, Desorption isotherms of tropical foodstuff, Application to banana, mango and pineapple, Drying Technology 23 (2005), 1477-1498.

[8] Y. Jannot and P. Meukam, Simplified estimation method for the determination of the thermal effusivity and thermal conductivity using a low cost hot strip, Measurements Sciences and Technology 15 (2004), 1932-1938.

[9] J. M. Hernandez, Séchage du chêne, caractérisation, procédés convectif et sous vide, PhD, Université Bordeaux 1, 1991.

[10] Y. Jannot and D. Lasseux, Etude d'un perméamètre pour plaques de faible perméabilité, Rapport d'étude, Contrat TREFLE/EDF, 2004.

[11] G. M. Jenkins and D. G. Watts, Spectral Analysis and its Applications, Holden-Day, 1968.

[12] M. Nakano and T. Miyazaki, The diffusion and nonequilibrium thermodynamic equations of water vapour in soils under temperature gradients, Soil Science 128 (1979), 184-188.

[13] E. Palomo del Barrio, Transport couplé de masse et de chaleur dans des parois en bois massif, Rapport Interne TREFLE, 2006.

[14] L. F. Shampine, M. W. Reichelt and J. A. Kierzenka, Solving index-1 DAEs in Matlab and Simulink, SIAM Review 41 (1999), 538-552.

[15] E. Palomo del Barrio, Roof components models simplification via statistical linearization and model reduction techniques, Energy and Buildings 29 (1999), 259-281.

[16] E. Palomo del Barrio, Résolution de problèmes thermiques de grande dimension, Méthodes de réduction, Editions Universitaires Européennes, 2011.

[17] E. C. Antoulas, An overview of approximation methods for large-scale dynamical systems, Annual Reviews in Control 29 (2005), 181-190.

[18] M. S. Smirnov, A system of differential equations of the drying process, J. Engng. Phys. 4 (1961), 40-44.

[19] M. D. Mikhailov and M. N. Özisik, Unified Analysis and Solutions of Heat and Mass Diffusion, Dover Publications, New York, 1994.

[20] G. Lefebvre, La méthode modale en thermique, Modélisation, simulation, mise en oeuvre et applications, Ellipses, Paris, 2007.

[21] B. C. Moore, Principal components analysis in linear systems: controllability, observability and model reduction, IEEE Trans. of Automatic Control AC-26 (1981), 17-31.

[22] A. Ait-Yahia and E. Palomo del Barrio, Thermal systems modelling via singular value decomposition: direct and modular approach, Applied Mathematical Modelling 23 (1999), 447-468.

[23] A. Ait-Yahia and E. Palomo del Barrio, Numerical simplification method for state-space models of thermal systems, Numerical Heat Transfer, Part B 37 (2000), 201-225.

[24] R. Bartels and G. Stewart, Solution of the matrix equation AX + XB = C: Algorithm 432, Comm. ACM 15 (1972), 820-826.

[25] S. Hammarling, Numerical solution of the stable, non-negative definite Lyapunov equation, IMA J. Numer. Anal. 2 (1984), 303-323.

[26] I. M. Jaimoukha and E. M. Kasenally, Krylov sunspace methods for solving large Lyapunov equations, SIAM J. Numer. Anal. 31 (1994), 227-251.

This title is indexed in Scopus

ISSN 0973-5763

Reprinted from the

JP Journal of Heat and Mass Transfer
Volume 10, Number 1, 2014, pp 1-32

REDUCED MODELS FOR COUPLED HEAT AND MOISTURE TRANSFER SIMULATION IN WOOD WALLS

by

E. Palomo del Barrio, S. Raji,

M. Duquesne and A. Sempey

Pushpa Publishing House
Vijaya Niwas, 198 Mumfordganj
Allahabad 211002, INDIA
http://pphmj.com/journals/jphmt.htm
jphmt@pphmj.com & arun@pphmj.com

OUR PUBLICATIONS

1. Advances and Applications in Discrete Mathematics (GIF : 0.378)
2. Advances and Applications in Fluid Mechanics (GIF : 0.689 ; SCOPUS)
3. Advances and Applications in Statistics (GIF : 0.812)
4. Advances in Computer Science and Engineering (GIF : 0.705)
5. Advances in Differential Equations and Control Processes (GIF : 0.607)
6. Advances in Fuzzy Sets and Systems (GIF : 0.703)
7. Current Development in Oceanography (GIF : 0.587)
8. Far East Journal of Applied Mathematics (GIF : 0.727)
9. Far East Journal of Dynamical Systems (GIF : 0.685)
10. Far East Journal of Electronics and Communications (GIF : 0.701 ; SCOPUS)
11. Far East Journal of Mathematical Education (GIF : 0.604)
12. Far East Journal of Mathematical Sciences (FJMS) (GIF : 0.692 ; SCOPUS)
13. Far East Journal of Theoretical Statistics (GIF : 0.767)
14. JP Journal of Algebra, Number Theory & Applications (GIF : 0.681 ; SCOPUS)
15. JP Journal of Biostatistics (GIF : 0.581)
16. JP Journal of Fixed Point Theory and Applications (GIF : 0.624)
17. JP Journal of Geometry and Topology (GIF : 0.725 ; SCOPUS)
18. JP Journal of Heat and Mass Transfer (GIF : 0.604 ; SCOPUS)
19. International Journal of Functional Analysis, Operator Theory and Applications (GIF : 0.597)
20. International Journal of Materials Engineering and Technology (GIF : 0.801)
21. International Journal of Numerical Methods and Applications (GIF : 0.619)
22. Universal Journal of Mathematics and Mathematical Sciences (GIF : 0.564)
23. Surveys in Mathematics and Mathematical Sciences (GIF : 0.558)
24. International Journal of Nutrition and Dietetics

New Journals From 2014

25. Advanced Studies in Artificial Intelligence
26. Advances and Applications in Software Engineering
27. Journal of Advanced Studies in Telecommunications
28. Universal Journal of Applied Physics and Technology
29. Universal Journal of Economic and Business Management
30. Universal Journal of Electrical Engineering and Informatics
31. Universal Journal of Mechanical Sciences and Technology

Pushpa Publishing House, Vijaya Niwas, 198, Mumfordganj, Allahabad 211002, India

arun@pphmj.com www.pphmj.com